Supramolecular Chemistry Hot Paper

How to cite: *Angew. Chem. Int. Ed.* **2021**, *60*, 7617–7620
International Edition: doi.org/10.1002/anie.202016253
German Edition: doi.org/10.1002/ange.202016253

Boric Acid-Fueled ATP Synthesis by F_oF_1 ATP Synthase Reconstituted in a Supramolecular Architecture

Xia Xu, Jinbo Fei, Youqian Xu, Guangle Li, Weiguang Dong, Huimin Xue, and Junbai Li**

Abstract: *Significant strides toward producing biochemical fuels have been achieved by mimicking natural oxidative and photosynthetic phosphorylation. Here, different from these strategies, we explore boric acid as a fuel for tuneable synthesis of energy-storing molecules in a cell-like supramolecular architecture. Specifically, a proton locked in boric acid is released in a modulated fashion by the choice of polyols. As a consequence, controlled proton gradients across the lipid membrane are established to drive ATP synthase embedded in the biomimetic architecture, which facilitates tuneable ATP production. This strategy paves a unique route to achieve highly efficient bioenergy conversion, holding broad applications in synthesis and devices that require biochemical fuels.*

Bioinspired supramolecular chemistry has made a great impact on synthesizing specific molecules and constructing functional hierarchical architectures.[1] By mimicking natural mitochondrion or chloroplast, much attention has been paid to developing artificial systems for efficient bioenergy conversion.[2] As a directly-consumable bioenergy currency, adenosine triphosphate (ATP) plays critical roles in a wide range of bioactivities including mass transportation, signal transduction and biochemical synthesis.[3] In nature, it is mainly produced through oxidative phosphorylation and photophosphorylation. Up to now, significant advance in artificial production of ATP has been achieved in mitochondrion or chloroplast-like systems.[4] For instance, nanozyme-catalyzed cascade reactions were developed to mimic mitochondrion toward conversion of glucose into ATP.[5] In addition, photochemical reactions were coupled to yield ATP in synthetic chloroplasts.[6] However, few reports involve non-redox processes.[7] In general, a cross-membrane proton gradient is necessary driving force for ATP synthesis.[8] Thus, non-redox proton-generated processes could be integrated to achieve efficient ATP production in a well-defined system.

Boric acid ester, a typical dynamic chemical bond, has attracted increasing attention due to extensive applications in asymmetric organic synthesis, smart drug delivery and self-healing systems.[9] Polyols such as mannitol are utilized to form boric acid esters. Their physicochemical and biological properties can be modulated by molecule structures of polyols and boric acids. Most boric acid ester chemical processes produce water rather than proton.[10] The one releasing proton is the case of boric acid and polyols under ambient condition, although they are usually used for analytical chemistry.[11] Hence, it can be envisioned that this boric acid ester chemistry is utilized to generate proton gradients as the driving force for bioenergy conversion.

In this communication, we develop boric acid ester chemistry to controllably synthesize bioenergy molecules in a biomimetic supramolecular architecture by a non-redox route. The mechanistic basis is shown in Figure 1. Polyol triggers the release of proton locked in boric acid by generation of cyclic boronate esters. As a consequence, boric acid serves as the fuel to establish a proton gradient across a lipid bilayer supported by polyelectrolyte-assembled microcapsules. It drives embedded ATP synthase in the biomimetic architecture to produce biochemical fuel ATP from adenosine diphosphate (ADP) and inorganic phosphate (Pi).

To support soft proteoliposomes to form stable biomimetic supramolecular architecture, polyelectrolyte microcapsules were constructed via layer-by-layer technique by using microparticles as the removable template. The whole assembly process is revealed in Figure 2 a. The polyelectrolytes were chosen as typical shell materials of microcapsules because of their assembly ability through electrostatic interactions. In detail, manganese carbonate microparticles were prepared through simple chemical precipitation, which was analysed by employing scanning electron microscopy (SEM) and transmission electron microscopy (TEM). Figure S1 shows the mean size of manganese carbonate microparticles with rough surfaces is around 3 μm. Through purification, the charged polyelectrolytes (Figure S2a) were sequentially deposited on the surface of manganese carbonate microparticles through electrostatic interactions. Microcapsules were obtained after selective removal of manganese carbonate cores by using ethylenediaminetetraacetic acid disodium salt (EDTA-Na_2) under mild condition. These assembly processes were monitored by detecting the surface potentials (Figure S2b). After removing the core, the final PEI-$(PSS/PAH)_3$ microcapsules, with the similar diameter, possess the typical folded characterization (Figure S2c). The result is in good consistence with

[*] X. Xu, Prof. Dr. J. Fei, Dr. G. Li, W. Dong, H. Xue, Prof. Dr. J. Li
Beijing National Laboratory for Molecular Sciences (BNLMS), CAS Key Lab of Colloid, Interface and Chemical Thermodynamics, Institute of Chemistry, Chinese Academy of Sciences
100190 Beijing (China)
E-mail: feijb@iccas.ac.cn
jbli@iccas.ac.cn
X. Xu, Prof. Dr. J. Fei, H. Xue, Prof. Dr. J. Li
University of Chinese Academy of Sciences
100190 Beijing (China)
Prof. Dr. Y. Xu
Third Military Medical University
400038 Chongqing (China)
Supporting information and the ORCID identification number(s) for the author(s) of this article can be found under: https://doi.org/10.1002/anie.202016253.

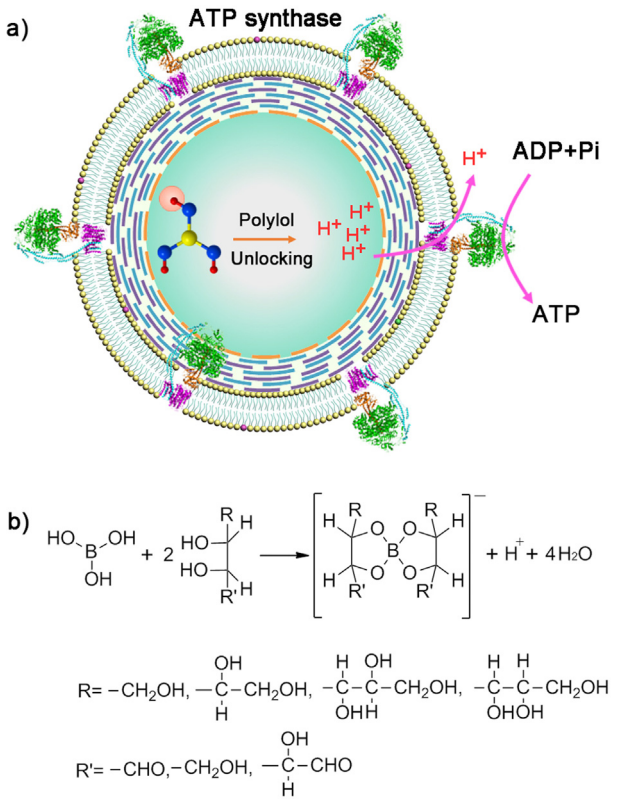

Figure 1. a) Schematic illustration of the supramolecular architecture, which is composed of polyelectrolyte microcapsule supporting ATP synthase (PDB: 6VON)-containing liposomes. With this biomimetic architecture, in the presence of polyols, a proton locked in boric acid is released to generate cross-membrane proton gradients, driving ATP synthase to transform ADP and Pi into ATP in a controlled fashion. b) The relevant boric acid ester chemical reaction.

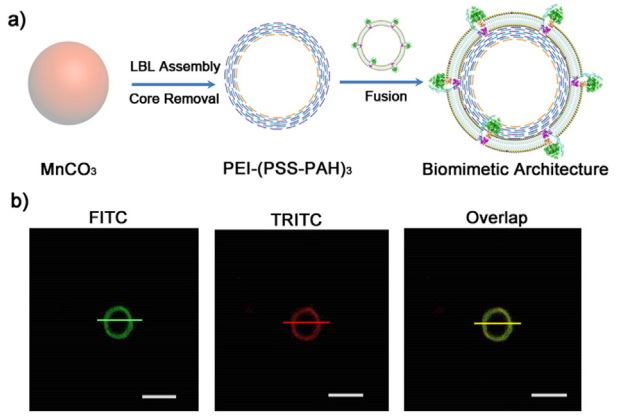

Figure 2. a) Schematic diagram of the supramolecular assembly of the biomimetic architecture. b) CLSM images of FITC-labeled microcapsules (left), TRITC-labeled proteoliposome (middle) and overlapping structure (right). The excitation wavelengths of FITC and TRITC are 405 nm and 561 nm, respectively (scale bars = 3 μm).

the previous reports.[12] These microcapsules can serve as the supporting substrate to enhance the stability of proteoliposomes.

After purified from chloroplast in fresh spinach through sucrose density gradient centrifugation, cF_oF_1-ATP synthase was identified by sodium dodecyl sulfate-polyacrylamide gel electrophoresis (SDS-PAGE). As revealed in Figure S3a, the subunits (α, β, γ, ε, δ, a, b, c) in the purified ATP synthase were present clearly, indicating the structure integrity.[13] Then, ATP synthase was reconstituted with mixed lipids (dimyristoyl phosphatidyl choline (DMPC) and dimyristoyl phosphatidylglycerole (DMPG), shown in Figure S3b) to form proteoliposomes, according to the reported method.[14] The activity of ATP synthase-containing proteoliposomes was detected by using a luciferin-luciferase assay (Figure S3c). The result suggests that purified ATP synthase is active and can be used for the next research. In addition, the protein content (4 mg mL^{-1}) was determined by utilizing coomassie bright blue (shown in Figure S4). Further, ATP synthase-containing proteoliposomes were co-incubated with dispersive microcapsules to construct the biomimetic architecture, as revealed in Figure 2a. To verify the successful spreading of the proteoliposomes on the surface of the microcapsules, confocal laser scanning microscopy (CLSM) was carried out to achieve visualization of components using green and red fluorescent probes. The homogeneously distributed and fully overlapped fluorescence intensity (Figure 2b and Figure S5) clearly indicates that the proteoliposomes were spread on the microcapsules surface to assemble the biomimetic microreactor. It results from microcapsule-mediated liposome fusion.[15]

Cross-membrane proton gradient is the driving force for ATP synthase to produce ATP. The general chemical reaction between boric acid and polyol is shown in Figure 3a. Under mild condition, boric acid is a weak acid ($pK_a = 5.8 \times 10^{-8}$). It means proton is at a locked state and stored in this molecule. In the presence of polyol, boric acid can be transformed into a stronger acid and proton is unlocked to release. To prove this, mannitol was utilized as a typical model in an unbuffered 1 mM boric acid solution. The product was characterized by low resolution electrospray ionization mass spectrometry

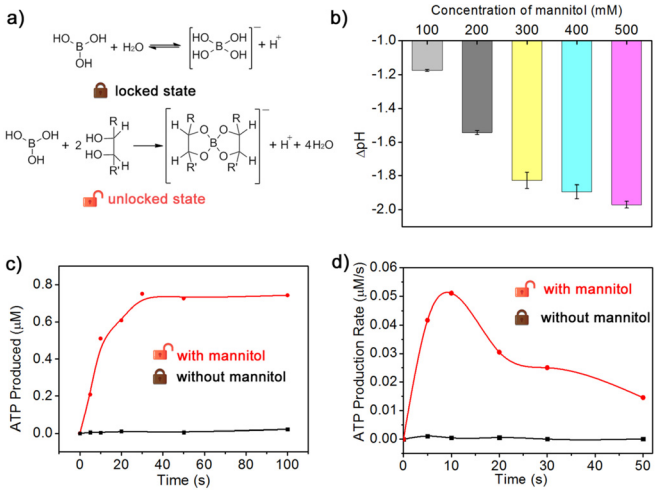

Figure 3. a) Chemical equilibria of boric acid with and without polyols. b) pH change of boric acid (1 mM) in the presence of different concentrations of mannitol (100, 200, 300, 400 and 500 mM). c) ATP synthesis by the assembled bioreactor a function of the reaction time with and without mannitol and d) the relevant ATP production rate.

(LR-ESI-MS). The ion peak at 371 appears in the mass spectrum (Figure S6), which can be assigned to the existence of the relevant boric acid ester. Figure 3b demonstrates that along with the increase of the concentration of mannitol, the pH value of the mixed solution has a greater decrease. It means pH change is proportional to the concentration of mannitol. These findings indicate that the boric acid ester chemistry can generate tuneable proton gradients by changing the concentration of mannitol. To be specific, there is pH decrease of 1.54 unit when the concentration of mannitol is 200 mM. It can be attributed to the ester reaction of mannitol and boric acid, shifting the equilibrium reaction of disassociation (Figure 3a). Based on these findings, we envision mannitol releases the proton bonded within boric acid to generate cross-membrane proton gradient, which can serve as the driving force for ATP production. Thus, boric acid and mannitol was introduced into the assembled architecture to investigate ATP production as a function of time. ATP was measured by using a luciferin-luciferase assay after immersion into a buffer solution with and without mannitol (Figure 3c). ATP production was obtained by using the standard curve (shown in Figure S7). It shows accompanying the introduction of mannitol, the concentration of produced ATP in the system increases and tends to a plateau of 0.74 μM at 30 s. Based on the relevant kinetic analyses in Figure 3d, the maximum average production rate is 0.05 $\mu M s^{-1}$ at 10 s. In contrast, there is no obvious ATP production in the absence of mannitol. These results demonstrate that mannitol enables boric acid as a proton fuel to drive ATP synthesis.

To confirm the simplicity and generality of this strategy above, we investigated other polyol-based systems. The chemical structures of typical polyols are shown in Figure 4a. As revealed in Figure 4b, after these polyols were introduced into the solution, there are obvious pH changes. In detail, after chemical re-equilibrium, for arabinose, the pH value of the solution is decreased by 0.35 unit, while for talose, the pH value went down by 1.17 unit. There is the highest decrease (1.40 unit) for ribose, as shown in Figure 4b. The above results reveal that polyols can release proton from boric acid as a proton source. Meanwhile, it seems the chemical structure of the polyols is a key factor and more structure-effect relationships need to be established to optimize the process. LR-ESI-MS results demonstrate the formation of borate ester between boric acid and these polyols, as shown in Figure S8–S10. Further, these boric acid ester systems were applied as proton fuel to produce ATP. To be specific, Figure 4c gives the relevant ATP production rates. For arabinose, the average ATP production rate is 0.0025 $\mu M s^{-1}$. For talose, it is 0.008 $\mu M s^{-1}$. In particular, it is the highest up to 0.028 $\mu M s^{-1}$ for ribose, which is comparable to those in natural oxidative phosphorylation and photophosphorylation. Moreover, this result is in good consistence of pH change above (Figure 4b), validating that greater proton gradient generates higher ATP production rate.

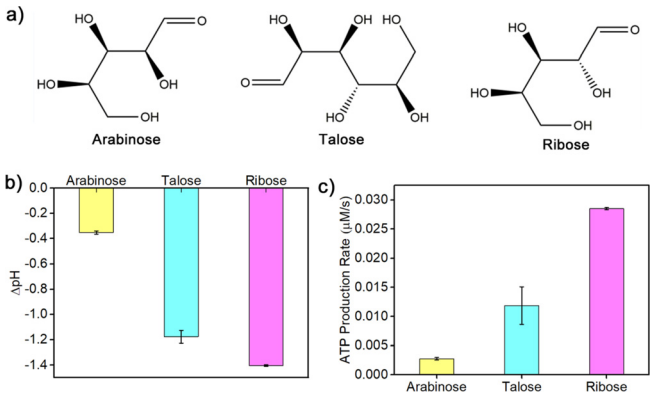

Figure 4. a) Chemical structures of typical polyols. b) pH changes after boric acid reacts with arabinose, talose and ribose. c) The relevant average ATP production rates.

Taken together, these findings above confirm the simplicity, generality and efficiency of this approach. Importantly, these polyols can be used for producing bioenergy by redox reactions in nature. This work provides a non-redox route to achieve their bioenergy conversion. Considering that intrinsic biocompatibility of these polyols and high efficiency of ATP production, the assembled bioreactor can be integrated with ATP-driven cascade reactions for cell-free protein synthesis and active transports based on motor protein-containing biodevices.

In summary, boric acid ester chemistry is explored to modulate bioenergy synthesis in a bioinspired supramolecular architecture. Polyols remarkably shift the disassociation equilibrium of boric acid, achieving a locked-to-unlocked state transformation of proton. Thus, proton release is triggered to generate a proton gradient across the lipid membrane, which serves as the driving force for bioenergy production. The production rate can be tuned by the choice of polyols. Under optimal conditions, the production rate of ATP is as high as 0.05 $\mu M s^{-1}$ when mannitol is used. This minimally robust supramolecular system integrates artificial and natural processes to achieve highly efficient biochemical transformation. This strategy can be extended to performing ATP-dependent biosynthesis and active transport.

Acknowledgements

The authors gratefully acknowledge the financial support for this research from the National Nature Science Foundation of China (No. 21961142022, 21872150 and 22072160). J.F. particularly thanks the Youth Innovation Promotion Association of CAS (No. 2016032) and Institute of Chemistry, CAS (No. Y6290512B1).

Conflict of interest

The authors declare no conflict of interest.

Keywords: biochemical fuel · biomimetic architectures · biosynthesis · proton gradients · supramolecular assembly

[1] a) K. Ariga, Q. M. Ji, T. Mori, M. Naito, Y. Yamauchi, H. Abe, J. P. Hill, *Chem. Soc. Rev.* **2013**, *42*, 6322–6345; b) B. C.

Buddingh', J. C. M. van Hest, *Acc. Chem. Res.* **2017**, *50*, 769 – 777; c) M. Komiyama, K. Yoshimoto, M. Sisido, K. Ariga, *Bull. Chem. Soc. Jpn.* **2017**, *90*, 967 – 1004; d) N. Carlsson, H. Gustafsson, C. Thorn, L. Olsson, K. Holmberg, B. Akerman, *Adv. Colloid Interface Sci.* **2014**, *205*, 339 – 360; e) S. M. Chen, H. L. Gao, Y. B. Zhu, H. B. Yao, L. B. Mao, Q. Y. Song, J. Xia, Z. Pan, Z. He, H. A. Wu, S. H. Yu, *Nat. Sci. Rev.* **2018**, *5*, 703 – 714; f) C. S. Hawes, T. Gunnlaugsson, *Chem* **2017**, *2*, 463 – 465; g) Y. Cui, J. Fei, J. Li, *Sci. China Chem.* **2011**, *41*, 273 – 280; h) L. Gao, Y. Zhang, L. Zhao, W. Niu, Y. Tang, F. Gao, P. Cai, Q. Yuan, X. Wang, H. Jiang, X. Gao, *Sci. Adv.* **2020**, *6*, eabb142; i) K. Ariga, X. Jia, J. Song, J. P. Hill, D. T. Leong, Y. Jia, J. Li, *Angew. Chem. Int. Ed.* **2020**, *59*, 15424 – 15446; *Angew. Chem.* **2020**, *132*, 15550 – 15574; j) B. Roy, T. Govindaraju, *Bull. Chem. Soc. Jpn.* **2019**, *92*, 1883 – 1901.

[2] a) G. Li, J. Fei, Y. Xu, Y. Li, J. Li, *Adv. Funct. Mater.* **2018**, *28*, 1706557; b) X. Feng, Y. Jia, P. Cai, J. Fei, J. Li, *ACS Nano* **2016**, *10*, 556 – 561; c) G. Steinberg-Yfrach, J. L. Rigaud, E. N. Durantini, A. L. Moore, D. Gust, T. A. Moore, *Nature* **1998**, *392*, 479 – 482; d) L. Zhao, Y. Liu, R. Xing, X. Yan, *Angew. Chem. Int. Ed.* **2020**, *59*, 3793 – 3801; *Angew. Chem.* **2020**, *132*, 3821 – 3829; e) J. Han, K. Liu, R. Chang, L. Zhao, X. Yan, *Angew. Chem. Int. Ed.* **2019**, *58*, 2000 – 2004; *Angew. Chem.* **2019**, *131*, 2022 – 2026; f) Y. Li, Q. Zou, C. Yuan, S. Li, R. Xing, X. Yan, *Angew. Chem. Int. Ed.* **2018**, *57*, 17084 – 17088; *Angew. Chem.* **2018**, *130*, 17330 – 17334.

[3] a) H. J. Choi, C. D. Montemagno, *Nano Lett.* **2005**, *5*, 2538 – 2542; b) Y. Xu, J. Fei, G. Li, T. Yuan, X. Xu, J. Li, *Angew. Chem. Int. Ed.* **2019**, *58*, 5572 – 5576; *Angew. Chem.* **2019**, *131*, 5628 – 5632; c) L. Otrin, N. Marusic, C. Bednarz, T. Vidakovic-Koch, I. Lieberwirth, K. Landfester, K. Sundmacher, *Nano Lett.* **2017**, *17*, 6816 – 6821.

[4] a) O. Gutiérrez-Sanz, P. Natale, I. Marquez, M. C. Marques, S. Zacarias, M. Pita, I. A. Pereira, I. Lopez-Montero, A. L. De Lacey, M. Velez, *Angew. Chem. Int. Ed.* **2016**, *55*, 6216 – 6220; *Angew. Chem.* **2016**, *128*, 6324 – 6328; b) S. Berhanu, T. Ueda, Y. Kuruma, *Nat. Commun.* **2019**, *10*, 1325; c) T. E. Miller, T. Beneyton, T. Schwander, C. Diehl, M. Girault, R. McLean, T. Chotel, P. Claus, N. S. Cortina, J. Baret, T. J. Erb, *Science* **2020**, *368*, 649 – 654; d) K. Y. Lee, S. J. Park, K. A. Lee, S. H. Kim, H. Kim, Y. Meroz, L. Mahadevan, K. H. Jung, T. K. Ahn, K. K. Parker, K. Shin, *Nat. Biotechnol.* **2018**, *36*, 530 – 535.

[5] P. Schwille, J. Spatz, K. Landfester, E. Bodenschatz, S. Herminghaus, V. Sourjik, T. J. Erb, P. Bastiaens, R. Lipowsky, A. Hyman, P. Dabrock, J. C. Baret, T. Vidakovic-Koch, P. Bieling, R. Dimova, H. Mutschler, T. Robinson, T. D. Tang, S. Wegner, K. Sundmacher, *Angew. Chem. Int. Ed.* **2018**, *57*, 13382 – 13392; *Angew. Chem.* **2018**, *130*, 13566 – 13577.

[6] a) Y. Xu, J. Fei, G. Li, T. Yuan, J. Li, *ACS Nano* **2017**, *11*, 10175 – 10183; b) Y. Li, X. Feng, A. Wang, Y. Yang, J. Fei, B. Sun, Y. Jia, J. Li, *Angew. Chem. Int. Ed.* **2019**, *58*, 796 – 800; *Angew. Chem.* **2019**, *131*, 806 – 810; c) Y. Jia, M. Xuan, X. Feng, L. Duan, J. Li, J. Li, *Chin. J. Chem.* **2020**, *38*, 123 – 129.

[7] G. Li, J. Fei, Y. Xu, B. Sun, J. Li, *Angew. Chem. Int. Ed.* **2019**, *58*, 1110 – 1114; *Angew. Chem.* **2019**, *131*, 1122 – 1126.

[8] P. Mitchell, *Nature* **1961**, *191*, 144 – 148.

[9] a) J. Yu, J. Wang, Y. Zhang, G. Chen, W. Mao, Y. Ye, A. R. Kahkoska, J. B. Buse, R. Langer, Z. Gu, *Nat. Biomed. Eng.* **2020**, *4*, 499 – 506; b) J. Wu, R. M. Bar, L. Guo, A. Noble, V. K. Aggarwal, *Angew. Chem. Int. Ed.* **2019**, *58*, 18830 – 18834; *Angew. Chem.* **2019**, *131*, 19006 – 19010; c) B. Josephson, C. Fehl, P. G. Isenegger, S. Nadal, T. H. Wright, A. W. J. Poh, B. J. Bower, A. M. Giltrap, L. Chen, C. Batchelor-McAuley, G. Roper, O. Arisa, J. B. I. Sap, A. Kawamura, A. J. Baldwin, S. Mohammed, R. G. Compton, V. Gouverneur, B. G. Davis, *Nature* **2020**, *585*, 530 – 537.

[10] a) A. Lopalco, A. A. Lopedota, V. Laquintana, N. Denora, V. J. Stella, *J. Pharm. Sci.* **2020**, *109*, 2375 – 2386; b) Y. Suzuki, D. Kusuyama, T. Sugaya, S. Iwatsuki, M. Inamo, H. D. Takagi, K. Ishihara, *J. Org. Chem.* **2020**, *85*, 5255 – 5264.

[11] M. Kijewska, A. Czerwinska, S. Al-Harthi, G. Wolczanski, M. Waliczek, A. H. Emwas, M. Jaremko, L. Jaremko, P. Stefanowicz, Z. Szewczuk, *Chem. Commun.* **2020**, *56*, 8814 – 8817.

[12] L. Duan, Q. He, K. Wang, X. Yan, Y. Cui, H. Möhwald, J. Li, *Angew. Chem. Int. Ed.* **2007**, *46*, 6996 – 7000; *Angew. Chem.* **2007**, *119*, 7126 – 7130.

[13] W. Qi, L. Duan, K. W. Wang, X. H. Yan, Y. Cui, Q. He, J. Li, *Adv. Mater.* **2008**, *20*, 601 – 605.

[14] P. Turina, D. Samoray, P. Gräber, *EMBO J.* **2003**, *22*, 418 – 426.

[15] Y. Xu, J. Fei, G. Li, T. Yuan, Y. Li, C. Wang, X. Li, J. Li, *Angew. Chem. Int. Ed.* **2017**, *56*, 12903 – 12907; *Angew. Chem.* **2017**, *129*, 13083 – 13087.

Manuscript received: December 7, 2020
Accepted manuscript online: December 27, 2020
Version of record online: February 25, 2021

